Hindawi
Advances in Civil Engineering
Volume 2019, Article ID 1604208, 10 pages
https://doi.org/10.1155/2019/1604208

*Research Article*

# Seismic Behaviour of Straight-Tenon Wood Frames with Column Foot Damage

**Shengcai Li**,[1,2] **Zhijun Jiang**,[1] **Hongzhen Luo**,[1] **and Lei Zhang**[1]

[1]*School of Architectural Science and Civil Engineering, Yangzhou University, Yangzhou 225127, China*
[2]*CNR-IVALSA, Via Madonna del Piano 6, 50019 Sesto Fiorentino, Italy*

Correspondence should be addressed to Zhijun Jiang; jiangzj@yzu.edu.cn

Received 11 October 2018; Accepted 10 December 2018; Published 3 January 2019

Academic Editor: Rosario Montuori

Copyright © 2019 Shengcai Li et al. This is an open access article distributed under the Creative Commons Attribution License, which permits unrestricted use, distribution, and reproduction in any medium, provided the original work is properly cited.

Timber buildings might incur damages after a long service, because column foot damage affects the structural performance under the continued use. In this paper, six straight-tenon joint wood frame specimens were prepared with varying degrees of two different damage conditions at a scale of 1 : 3.52. To obtain failure mode and hysteresis performance of the specimens, the low-cycle reciprocating loading test was conducted. The stiffness degradation curves and equivalent viscous damping curves of the damaged wood frames were also analysed. The mechanical characteristics of the wood frames with column foot damage under the low-cycle reciprocating load were then simulated using the finite element method, and the results were compared to the test results. It is determined that as the degree of column foot damage increases, the fullness and peak of the hysteresis curves for wood frames, the equivalent viscous damping coefficients, and the overall seismic behaviour of the wood frame all gradually decrease. The skeleton curves obtained by finite element analysis and tests showed good agreement, verifying the influence of column foot damage on the seismic behaviour of ancient wood frame structures.

## 1. Introduction

The ancient wood-framed building is a masterpiece of Chinese traditional construction and has been considered an important part of the architectural cultural heritage in China. According to investigation of structural damage in recent earthquakes, the wood-framed building exhibits excellent seismic behaviour. Therefore, extensive research has been conducted to reveal the seismic mechanism of the wood-framed building. Research findings have obtained the degradation laws of hysteretic behaviour, restoring the force model and collapsing process simulations of timber structures under dynamic loading [1–3]. The mortise-tenon joints are important energy-consuming components. To explore the mechanical property of the mortise-tenon joint, Chinese traditional mortise-tenon jointed timber frames were tested under the monotonic or cyclic loading test to acquire its skeleton curve characteristics, degradation laws of rotational stiffness, failure mode, energy dissipation capacity, and mathematical model of hysteresis curve [4–9]. As a typical feature of the Chinese ancient timber building, Dou-Gong brackets can reduce the magnitude of earthquake forces significantly [10]. Chen et al. conducted experimental research on the structural performance of Dou-Gong brackets in terms of the load-carrying capacity, stiffness, and the failure modes under vertical load [11].

The timber column is a critical component of the structural system of these ancient wood-framed buildings. Research findings have revealed the unique role of the column-to-foundation joint, in which the column foot is unrestrained and laid flat on the foundation stone, providing seismic isolation and damping, reflecting the seismic approach of ancient wood-framed structures in "combining stiffness and flexibility, restraining hardness with softness, slipping seismic isolation, energy dissipation, and seismic mitigation." Wang et al. found that in a structure in which the timber column is unrestrained and laid flat on the foundation, forming a column foot joint between superstructure and stylobate, the column will only be subject to compression, experiencing no tension [12]. Qin et al. conducted a field experiment to demonstrate that the rotational stiffness of the column footing joint has notable influence on

the dynamic characteristics of the traditional Chinese timber structure [13]. Yao and Zhao constructed a friction-slipping seismic isolation model for a column and foundation stone by conducting an in-depth study of the friction-slipping seismic isolation mechanism present in the foundations of wood-framed ancient buildings and provided judging criteria for the slipping of the column foot [14]. He and Wang studied the rotational behaviour of the column foot during the rocking process accounting for the compression effect and proposed a theoretical restoring moment model for the column foot joint [15]. The relationship between the column foot corner and restoring moment for the column was determined through the press tests of the column foot according to Lee et al. [16].

These ancient wood-framed structures are generally vulnerable to deterioration in material and structural properties due to the effects of wind and rain, earthquakes, and artificial damage. Research findings have demonstrated that the fungi can cause significant losses in both wood weight and strength [17]. Because the timber column is typically in direct contact with the masonry foundation and brickwork, it tends to be more susceptible to the effects of dampness and deterioration, resulting in reduced material strength and stiffness of the column section, which in turn sharply reduces the structural safety level of the ancient wood-framed building. Despite the implications of this issue, very few studies have investigated the impact of a damaged timber column on the seismic behaviour of a wood-framed structure. Accordingly, in the present study, a series of straight-tenon wood frames were constructed to investigate the impact of timber column foot damage on the seismic behaviour of the overall frame.

## 2. Materials and Methods

*2.1. Preparation of Specimens.* With reference to the specifications recorded in Yingzao Fashi (Treatise on Architectural Methods) of the Song Dynasty [18], six wood-framed specimens containing single-storey straight-tenon joints were constructed in two groups at a scale of 1 : 3.52, determined by a ratio of 1 cm to 2 Fen-II (where Fen-II is the unit length of Grade II material in the Song Dynasty, equal to 1.76 cm). The specimens were handmade by carpenters according to traditional practice, with each specimen as shown in Figure 1. The dimensions of the structural components in the straight-tenon wood frame models are provided in Table 1. These specimens were made of Los Angeles Douglas fir and were naturally dried for half a year. To facilitate the process of applying horizontal loads, the column head section in the proposed model was placed 200 mm above the top face of the beam column.

Two types of column foot deterioration were investigated: unilateral deterioration at the column foot (as shown in Figure 2) and circumferential deterioration at the column foot (see Figure 3). Based on the aforementioned types of damage, the specimens with artificial damages at both the column feet which show similar structural properties were simulated, designed, and prepared (see Figure 4). Three degrees of damage were determined through the ratio

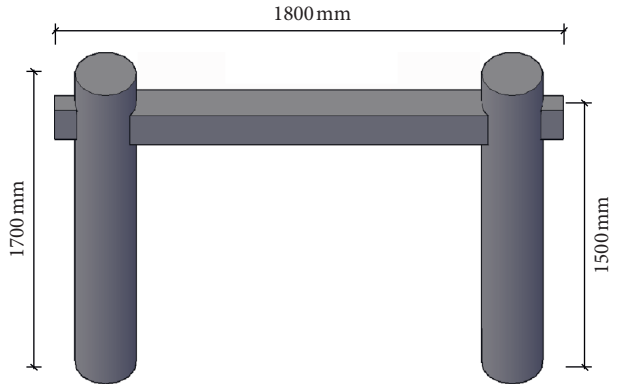


Figure 1: Straight-tenon wood frame model.

Table 1: Original dimensions of components and model dimensions.

| Specimen | Parameter | The Song Dynasty unit (Fen) | Model dimension (mm) |
|---|---|---|---|
| Column | Diameter of column | 42 | 210 |
| | Height of column | 300 | 1500 |
| Penetrating architrave | Length of architrave | 360 | 1800 |
| | Width of architrave | 24 | 120 |
| | Height of architrave | 36 | 180 |
| Straight-tenon joint | Length of tenon joint | 50 | 250 |
| | Width of tenon joint | 12 | 60 |
| | Height of tenon joint | 36 | 180 |

Figure 2: Unilateral column foot damage.

Figure 3: Circumferential column foot damage.

(a)

(b)

Figure 4: Models with artificial damage at the column foot. (a) Unilateral damage. (b) Circumferential damage.

of the actual bearing area between the bottom face of column foot and the column base $S_1$ to the original section area of column at the column foot $S_2$. The ratios were set as 1/5, 2/5, and 3/5, respectively, to explore the effect of varying degrees of damage on the structural performance. The original column bottom area $S_2$ of the specimens was determined according to the dimensions given in Table 1; thus, the values of $S_1$ can be determined for different degrees of damage. The artificial damage height at the column foot was taken as 200 mm. The dimensions of the models with unilateral and circumferential column foot damages are given in Tables 2 and 3, respectively.

*2.2. Loading Device.* In Figure 5, the test loading device is depicted. The column foot of the wood frame was unrestrained and laid flat on the foundation. With reference to actual loads on wood-framed buildings, according to the similarity relationship, a static vertical load of 50 kN was applied by a hydraulic jack to the two column heads using an I-shaped load sharing beam. To address the difficulty of consistently applying this vertical load as the wood frame moved horizontally over the course of the displacement test, a horizontal slip device was installed between the hydraulic jack and the reaction frame. The lateral loading was applied by a horizontal hydraulic servo actuator that was securely fixed to the reaction wall, and the relevant displacement data were automatically acquired by the experiment system.

Table 2: Dimensions of the model with unilateral column foot damage.

| Damage height (mm) | Damage depth (mm) | No. |
|---|---|---|
| 200 | 40 | ZJJ40 |
| | 80 | ZJJ80 |
| | 105 | ZJJ105 |

Table 3: Dimensions of the model with circumferential column foot damage.

| Damage height (mm) | Damage external diameter (mm) | Damage internal diameter (mm) | No. |
|---|---|---|---|
| 200 | 210 | 133 | ZGW133 |
| | | 163 | ZGW163 |
| | | 188 | ZGW188 |

*2.3. Loading Plan.* With reference to the ISO 16670 loading procedure, the lateral loading was controlled by displacement at a rate of 5 mm/s. The maximum lateral displacement under test control was 100 mm. The loading plan is shown in Figure 6. The loading was conducted in two stages. Stage 1: one loading cycle each was conducted to 1%, 3%, 5%, and 10% of the maximum displacement without stopping. Stage 2: three step-by-step loading cycles were conducted to 20%, 40%, 60%, 80%, and 100% of the maximum displacement in sequence.

## 3. Test Results and Analysis

Under the low-cycle reciprocating lateral loading plan, the six wood-framed models with deterioration at the column foot exhibited similar structural responses:

(1) During the initial stage of test loading sequence, a gap was observed between the straight-tenon joint and the mortise that, with the application of lateral displacement, began to gradually compress to produce a squeaking sound. The wood frame was observed to slightly rock.

(2) As the applied lateral displacement increased, the wood frame made a slight "flapping" noise from time to time, the column foot uplifted, and the column body began to obviously rock (see Figures 7(a) and 8(a)). During the column rocking process, the column foot alternately rotated leftwards and rightwards.

(3) When the applied lateral displacement reached 80 mm and 100 mm, the compressive deformation between the tenon and the mortise was intensified, exhibiting a substantial degree of plastic deformation, and the continuous noise from the wood frame grew louder, local compression deformation occurred at the edge of the column foot, and partial warping and cracking were observed (see Figures 7(b) and 8(b)).

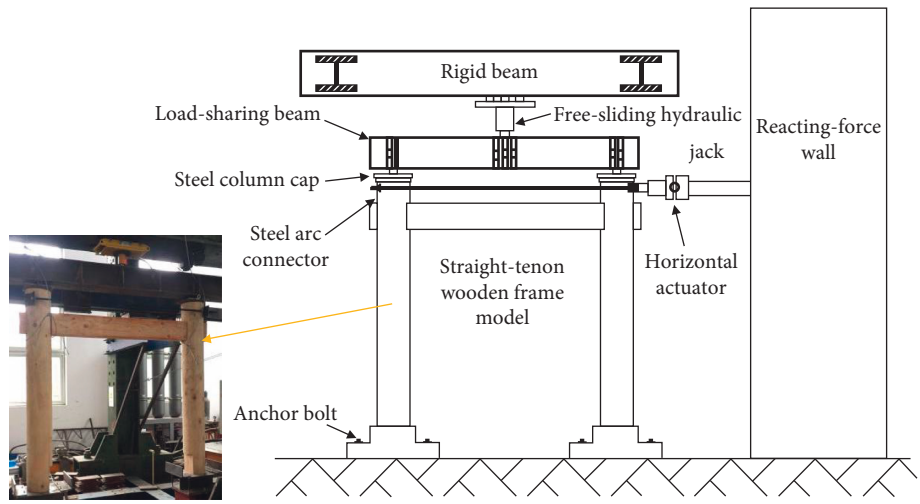


Figure 5: Test loading device.

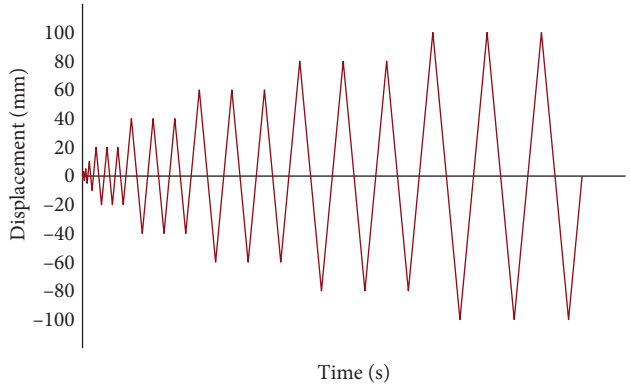


Figure 6: Test loading plan.

(4) At the end of the test loading sequence, it was found that there were generally traces of compressive forces on the bottom face of the column foot, and obvious compression deformation was observed symmetrically along two opposite edges on the bottom face of the column foot.

*3.1. Hysteresis Curves.* Research findings have revealed the unique role of the hysteresis curves in reflecting the seismic behaviour of wood frame [19–21]. Using the data acquired from the tests, the force-displacement ($P$-$\Delta$) hysteresis curves for two wood frame models, one with a unilaterally and another with a circumferentially damaged column foot, were obtained as shown in Figures 9 and 10, respectively. The $P$-$\Delta$ hysteresis curves for the two wood frame models are inversely $Z$-shaped, indicating that the wood frames with damaged column feet slipped. However, when the applied displacement is small, the hysteresis curves tend to develop linearly and show no significant residual deformation after unloading. This can be explained by the larger available compression area of the column foot, resulting in a compressive stress on the column foot smaller than the compressive strength of the wood fibres such that the deformation was basically maintained within the elastic range. As the applied displacement increases, the hysteresis curve develops nonlinearly, and the envelope area increases. This can be attributed to the occurrence of residual deformation and wood warping at the column foot as a result of the reduced compression area and the movement of high stress to the edges of the column foot. As the applied displacement further increases, the compression area is concentrated at the edges of the column foot, and the hysteresis curves tend to be full.

The hysteresis curves for the forward and reverse loading of the wood frame were basically symmetrical, indicating that the deformation performance of the wood frame during reciprocating movement was generally consistent. By comparing the hysteresis curves of the three wood frame specimens with the different degrees of the same column foot damage, it was found that the smaller the degree of damage to the column foot, the larger the area contained by the hysteresis curve, and the greater the peak load resisted. This is due to the fact that the smaller the degree of damage on the column foot, the larger the initial radius of column rotation around the foot section, and accordingly, under conditions of the same lateral displacement, there is a more significant embedment effect [22] at edges of the column foot, making the column behave in a more fixed manner.

*3.2. Stiffness Degradation.* Under the lateral load, the stiffness of the wood frames decreased with increasing applied displacement and applied cycles, resulting in stiffness degradation. The secant stiffness for each level of applied displacement can be calculated as follows:

$$K_i = \frac{|+F_i| + |-F_i|}{|+\Delta_i| + |-\Delta_i|}, \quad (1)$$

where for the $i$th applied displacement, $K_i$ is the lateral stiffness of the specimen, $F_i$ is the lateral resistance, and $\Delta_i$ is the applied displacement.

(a) (b)

Figure 7: Column foot behaviour in wood frame ZJJ40. (a) Uplift. (b) Edges with compression deformation.

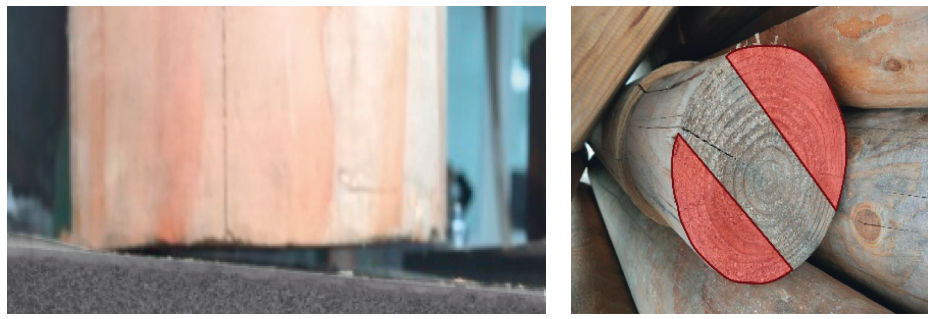

(a) (b)

Figure 8: Column foot behaviour in wood frame ZGW188. (a) Uplift. (b) Edges with compression deformation.

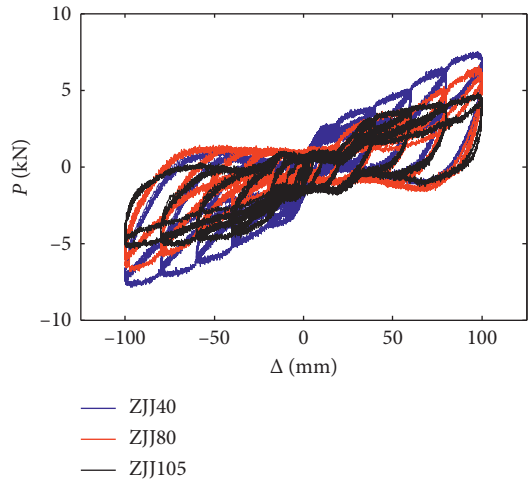


Figure 9: $P$-Δ hysteresis curve for unilateral column foot damage (ZJJ).

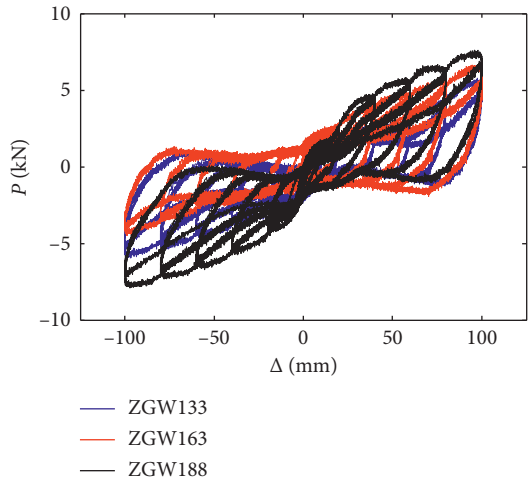


Figure 10: $P$-Δ hysteresis curve for circumferential column foot damage (ZGW).

Figures 11(a) and 11(b) show the stiffness degradation curves for the wood frames with unilateral and circumferential column foot damage, respectively. In Figure 11, as the applied displacement increases, the stiffness of the wood frame sharply decreases, and when the applied displacement is largest, the stiffness decreases. The observed reduction in the stiffness of the wood frame was mainly the result of changes in the location of the reaction force on the column foot. As the applied displacement increases, the compression area of the column foot gradually decreases and the reaction force on the column foot moves to the edge of the foot, resulting in an increase in the restoring moment. In this case,

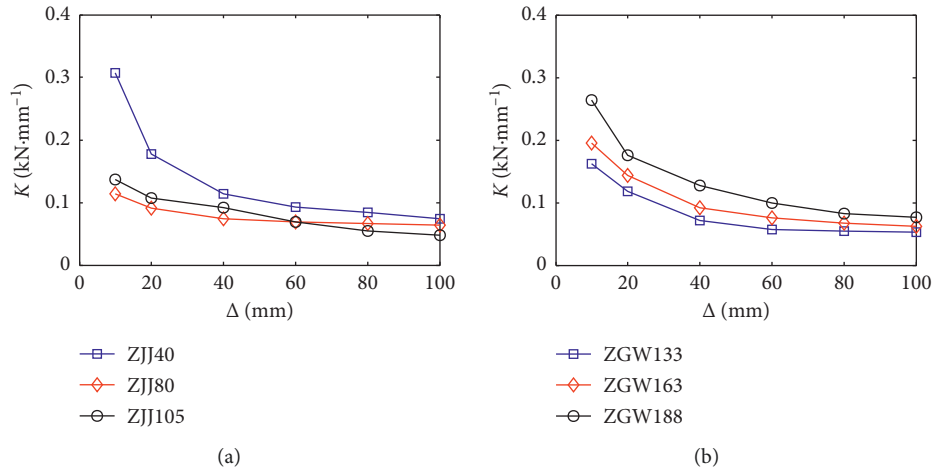


Figure 11: Stiffness degradation curves. (a) Unilateral column foot damage (ZJJ). (b) Circumferential column foot damage (ZGW).

the offset of the reaction force led to rapid increase in the restoring moment of the column foot and a higher rotational stiffness of the column foot. As the compression face moved closer to the edge of the column foot, these changes no longer led to an increase in the restoring moment, and the rotational stiffness gradually decreased, resulting in stiffness degradation. Additionally, the plastic deformation caused by the reciprocating movement of the wood frame also resulted in reduced rigidity of the wood frame.

By comparing the stiffness degradation curves for the wood frames with the same type of column foot damage, it is clear that the larger the damaged area of the column foot section, the less rigid the wood frame overall. In addition, it has been considered that the greater the distance between the location of the reaction force on the column foot and the section centre, the greater the restoring moment of the wood frame, resulting in greater rigidity.

*3.3. Energy Dissipation Capacity.* The energy dissipation capacity, which can be reflected by using of the equivalent viscous damping coefficients ($h_e$), was critical to evaluate the seismic behaviour for the wood frame [23]. The equivalent viscous damping coefficients of the wood frame specimens with the two types of column foot damage under the applied displacements are shown in Figure 12. Clearly, during the initial stage of the low-cycle reciprocating loading, the equivalent viscous damping coefficients of the wood frame specimens increase and peak at an applied displacement of 20 mm. This small deformation allowed for full contact between the structural components and also improved the material strength to some extent, thus increasing the energy dissipation of the wood frame system. As the applied displacement increases, the equivalent viscous damping coefficients significantly decrease, indicating that damage to the wood frame was gradually being accumulated, decreasing the energy dissipation capacity. Once the applied displacement exceeds 60 mm, the energy dissipation capacity continues to decrease, but to a much smaller degree. By comparing the energy dissipation of wood frames with the same type of column foot damage but with different degrees of damage, it can be determined that the smaller the degree of damage on the column foot, the larger the energy dissipation capacity of the wood frame.

## 4. Finite Element Analysis

To further examine the seismic behaviour of the wood frames with damaged column feet and to evaluate the practicability of numerically modelling for this behaviour, the low-cycle reciprocating loadings of the two types of experimentally evaluated damaged wood frames were simulated using the finite element method (FEM) analysis software package Abaqus, and the analytical results were compared to the experimentally observed results.

*4.1. FEM Model.* The construction of an accurate FEM model involves addressing certain critical problems such as the material properties, contact effects, and element form. The wood material properties were defined using parameters obtained from a material properties test. Given the orthotropy of wood material, the elastic modulus ($E$), shear modulus ($G$), and Poisson's ratio ($\gamma$) in the three orthogonal directions of the wood material were defined in the model. The values for the material constants used in this study are given in Table 4. The numbers 1, 2, and 3 denote three orthogonal directions. To reflect the complex mechanical behaviour of wood, the constitutive model of wood under parallel-to-grain and perpendicular-to-grain directions shown in equations (2) and (3) was used, respectively. And the equations (2) and (3) are depicted in Figure 13:

$$\sigma = \begin{cases} E_t\varepsilon, & 0 \le \varepsilon < \varepsilon_{tu}, \\ E_c\varepsilon, & \varepsilon_0 \le \varepsilon < 0, \\ E_c\varepsilon_{c0}, & \varepsilon_{cu} \le \varepsilon < \varepsilon_{c0}, \end{cases} \quad (2)$$

where $E_t$ and $E_c$ are the elastic moduli under compression and tension in the linear elasticity stage, respectively, $\varepsilon_{c0}$ is the yield strain under compression, $\varepsilon_{cu}$ is the ultimate

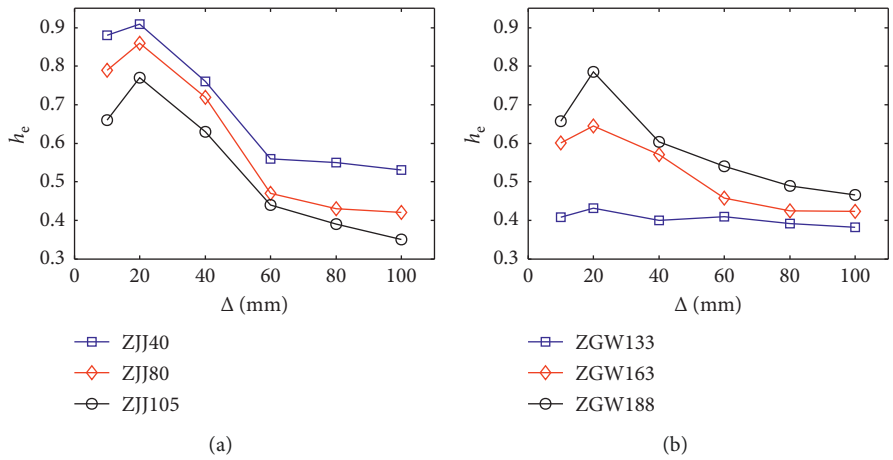


Figure 12: Energy dissipation curves for wood frame models. (a) Unilateral column foot damage (ZJJ). (b) Circumferential column foot damage (ZGW).

Table 4: Anisotropic parameters of Douglas fir timber.

| $E_1$ (Mpa) | $E_2$ (Mpa) | $E_3$ (Mpa) | $G_{12}$ (Mpa) | $G_{13}$ (Mpa) | $G_{23}$ (Mpa) | $\gamma_1$ | $\gamma_2$ | $\gamma_3$ |
|---|---|---|---|---|---|---|---|---|
| 16400 | 1300 | 900 | 910 | 1180 | 79 | 0.63 | 0.43 | 0.37 |

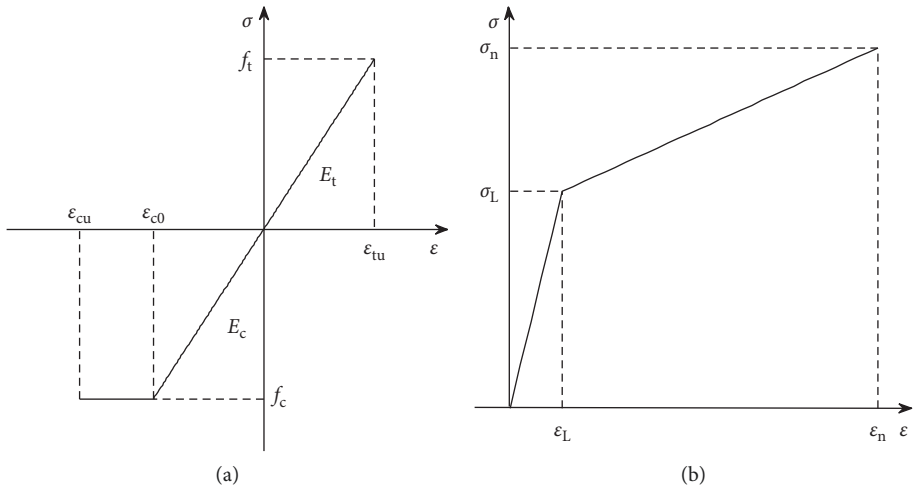


Figure 13: Stress-strain constitutive model for materials in the specimens. (a) Parallel-to-grain direction. (b) Perpendicular-to-grain direction.

compressive strain, $\varepsilon_{tu}$ is the ultimate tensile strain, $f_c$ is the compressive strength, and $f_t$ is tensile strength:

$$\sigma = \begin{cases} E_L \varepsilon, & 0 < \varepsilon \le \varepsilon_L, \\ \sigma_L + E_r(\varepsilon - \varepsilon_L), & \varepsilon_L < \varepsilon \le \varepsilon_n, \end{cases} \quad (3)$$

where $E_L$ and $E_r$ are the elastic moduli under compression in the linear elasticity stage and hardening stage, respectively; $\sigma_L$ is the maximum stress in the linear elasticity stage; $\sigma_n$ is the maximum stress in the hardening stage; $\varepsilon_L$ is the strain corresponding to $\sigma_L$; and $\varepsilon_n$ is the strain corresponding to $\sigma_n$.

To simulate the semirigid properties at the beam-column joints, the simulated components were made to be in general contact. To overcome shear self-locking and make the calculations more accurate, the C3D8I solid 3D element was used. For the mesh discretization of the model, element size of the foundation and other parts are 100 × 100 × 100 mm$^3$ and 30 × 30 × 30 mm$^3$, respectively. The completed FEM model that shows eventual partitions is shown in Figure 14.

*4.2. Results of FEM Model and Comparison with Experimental Test Results.* Skeleton curves characterize the relationship between the restoring force and the deformation characteristics of wood frames under low-cycle reciprocating loading, providing an important representation of the seismic behaviour. A comparison between skeleton curves of the test and the numerical simulation results is shown in Figures 15 and 16.

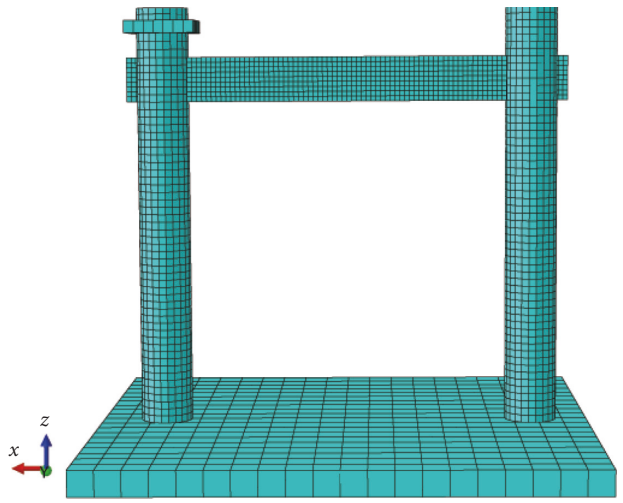


Figure 14: FEM model of wood frame.

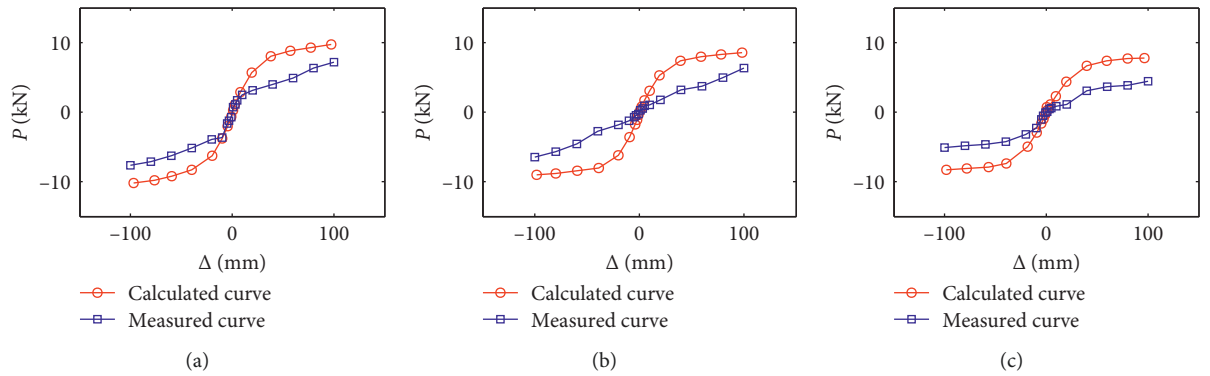


Figure 15: Comparison of experimentally determined and numerically simulated skeleton curves for unilateral column foot damage (ZJJ). (a) ZJJ40. (b) ZJJ80. (c) ZJJ105.

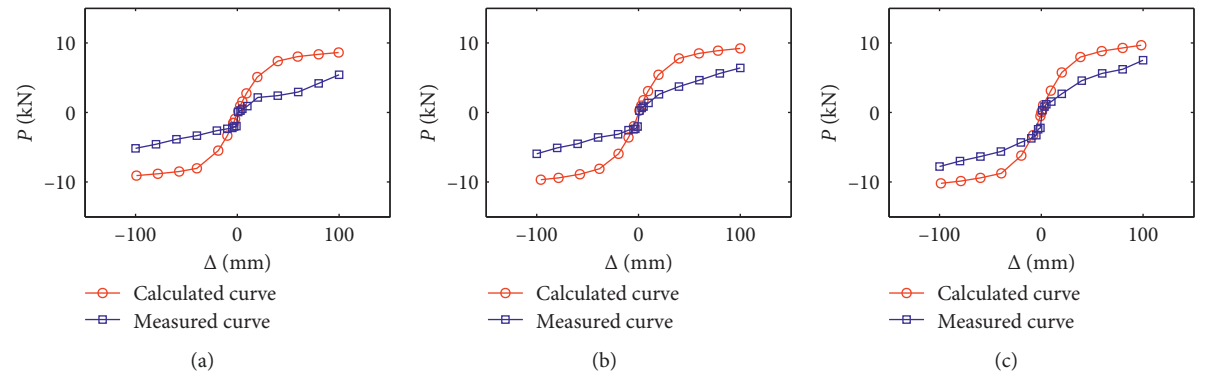


Figure 16: Comparison of experimentally determined and numerically simulated skeleton curves for circumferential column foot damage (ZGW). (a) ZGW133. (b) ZGW163. (c) ZGW188.

Certain differences between the FEM calculated and experimentally determined skeleton curves can be observed for wood frames with the two types of damage evaluated. These differences can be attributed to the following:

(1) Model dimension errors. The FEM model was constructed from data with no dimensional errors, but the construction process of the test model cannot be exact, and thus may include errors in fabrication and erection, causing certain dimensional discrepancies between the test model and the FEM model.

(2) Wood material property discrepancies. To construct the FEM model, parameters such as shear modulus

and Poisson's ratio were determined according to an empirical formula, and only the ultimate stress was used when defining the plasticity of the wood material, certainly resulting some departure from the actual wood properties.

(3) Loading differences at the column end. In the experiment, because the vertical load was applied on the column end by a hydraulic jack, distribution beam, and column cap, there was an obvious horizontal static friction between the column cap and the column end, which is a different condition than the boundary condition and loading arrangement in the FEM simulation.

(4) Randomness of wood material properties. In this test, only a small set of specimens were made to test individual conditions. Due to discreteness of wood material properties, the test results were therefore also very discrete, resulting in certain differences between the test results and the numerical simulation results, which assumed more universal properties.

Additionally, the observed gap between the tenon and mortise in the wood frame joints caused a large amount of slippage during the initial stage of the test resulted in the deformation of the tenon and led to a reduction in frame capacity, and the differences in the values for the tenon-mortise friction coefficient in the FEM simulation and in the test model also led to differences between the experimental and simulation results. Although these differences undeniably exist, a comparison of results demonstrates that the overall trend of the FEM results was basically consistent with that of the experimental results, indicating that the seismic behaviour of wood frames can be further examined with confidence using the FEM model.

## 5. Conclusions

In order to investigate the effects of column foot damage on the seismic response of ancient wood-framed buildings, a series of test frames were constructed according to ancient building specifications and tested by cyclic lateral loading. The responses of wood frames with different degrees and types of column foot damage were observed and compared to an FEM analysis of frame models to determine their behaviour and to evaluate the ability of FEM to accurately replicate this behaviour. The following conclusions were drawn:

(1) For wood frames with the same type of column foot damage, as the degree of damage increased, the fullness and peak of the hysteresis curves of the wood frames gradually decreased.

(2) For wood frames with the same type of column foot damage, the greater the degree of damage, the smaller the rigidity of the wood frame. As the applied displacement increased, the stiffness of the wood frames significantly decreased.

(3) During the loading process, the energy dissipation capacity of the wood frames first slightly increased then decreased rapidly. At larger applied displacements, the energy dissipation capacity decreased at a slower rate. For wood frames with the same type of column foot damage, the smaller the degree of damage, the higher the energy dissipation capacity and the better the seismic behaviour.

(4) The overall trend of the wood frame skeleton curves obtained using the FEM and from the tests was the same, confirming the influence of column foot damage on the seismic behaviour of wood frames.

The column feet of ancient wood-framed building can be easily damaged, and the greater the damage, the more significant the impact on the seismic behaviour of the wood frames as a whole. Therefore, having demonstrated the deleterious effects of column foot damage on these structures, it is now necessary to conduct intensive research on effective reinforcement and repair techniques for these structural details in order to better protect remaining ancient wood-framed buildings.

## Data Availability

The data used to support the findings of this study are available from the corresponding author upon request.

## Conflicts of Interest

The authors declare that there are no conflicts of interest regarding the publication of this paper.

## Acknowledgments

This paper was supported by the National Natural Science Foundation of China (Grant nos. 51478409 and 51338001), the State Administration of Foreign Experts Affairs (Grant no. GDT20183200375), and Program of 100 Foreign Experts in Jiangsu Province (Grant no. JSB2017029).

## References

[1] J. Y. Chen, T. Y. Li, Q. S. Yang, X. W. Shi, and Y. X. Zhao, "Degradation laws of hysteretic behaviour for historical timber buildings based on pseudo-static tests," *Engineering Structures*, vol. 156, pp. 480–489, 2017.

[2] X. Meng, Q. Yang, J. Wei, and T. Li, "Experimental investigation on the lateral structural performance of a traditional Chinese pre-Ming dynasty timber structure based on half-scale pseudo-static tests," *Engineering Structures*, vol. 167, pp. 582–591, 2018.

[3] T. Nakagawa and M. Ohta, "Collapsing process simulations of timber structures under dynamic loading I: simulations of two-story frame models," *Journal of Wood Science*, vol. 49, no. 5, pp. 392–397, 2003.

[4] Q. Chun, Z. Yue, and J. Pan, "Experimental study on seismic characteristics of typical mortise-tenon joints of Chinese southern traditional timber frame buildings," *Science China Technological Sciences*, vol. 54, no. 9, pp. 2404–2411, 2011.

[5] C. C. Chen, H. X. Qiu, and M. G. Xu, "Experimental study on flexural behavior of typical mortise-tenon joints,"

*Applied Mechanics and Materials*, vol. 578-579, pp. 160–163, 2014.

[6] L.-k. Chen, S.-c. Li, Y.-t. Wang et al., "Experimental study on the seismic behaviour of mortise-tenon joints of the ancient timbers," *Structural Engineering International*, vol. 27, no. 4, pp. 512–519, 2018.

[7] S. F. Jiang, M. H. Wu, S. L. Ma, and D. Y. Lin, "Structural stiffness identification of traditional mortise-tenon joints based on statistical process control chart," *Journal of Aerospace Engineering*, vol. 31, no. 5, article 04018066, 2018.

[8] H. Huang, Y. Wu, Z. Li, Z. Sun, and Z. Chen, "Seismic behavior of Chuan-Dou type timber frames," *Engineering Structures*, vol. 167, pp. 725–739, 2018.

[9] C. Emile, X. B. Song, Y. J. Wu, and K. Li, "Lateral performance of mortise-tenon jointed traditional timber frames with wood panel infill," *Engineering Structures*, vol. 161, pp. 223–230, 2018.

[10] D. P. Fang, S. Iwasaki, M. H. Yu, Q. P. Shen, Y. Miyamoto, and H. Hikosaka, "Ancient Chinese timber architecture. II: dynamic characteristics," *Journal of Structural Engineering*, vol. 127, no. 11, pp. 1358–1364, 2001.

[11] Z. Chen, E. Zhu, F. Lam, and J. Pan, "Structural performance of Dou-Gong brackets of Yingxian wood pagoda under vertical load—an experimental study," *Engineering Structures*, vol. 80, pp. 274–288, 2014.

[12] J. Wang, J. X. He, Q. S. Yang, and N. Yang, "Study on mechanical behaviors of column foot joint in traditional timber structure," *Structural Engineering and Mechanics*, vol. 66, no. 1, pp. 1–14, 2018.

[13] S. J. Qin, N. Yang, and D. Lu, "Rotational behavior of column footing joint and its effect on the dynamic characteristics of traditional Chinese timber structure," *Shock and Vibration*, vol. 2018, Article ID 9726852, 2018.

[14] K. Yao and H. T. Zhao, "Mechanism of friction slipping seismic isolation of column and column base of ancient buildings," *Engineering Mechanics*, vol. 23, no. 8, pp. 127–131, 2006, in Chinese.

[15] J. He and J. Wang, "Theoretical model and finite element analysis for restoring moment at column foot during rocking," *Journal of Wood Science*, vol. 64, no. 2, pp. 97–111, 2017.

[16] D. Lee, Y. Araki, T. Endo, N. Yoshida, and K. Uetani, "Modelling of column base for traditional timber buildings based on local compression experiments at contact surface between column base and foundation stone," *Journal of Structural and Construction Engineering (Transactions of AIJ)*, vol. 74, no. 639, pp. 865–872, 2009.

[17] J. J. Morrell and R. Zabel, "Wood strength and weight losses caused by soft rot fungi isolated from treated southern pine utility poles," *Wood and Fiber Science*, vol. 17, no. 1, pp. 132–143, 1985.

[18] J. Li, *Song Dynasty—Ying Zao Fa Shi (Treatise on Architectural Methods)*, The Commercial Press, Shanghai, China, 1954, in Chinese.

[19] J. Chen, Y. F. Chen, X. Shi, Y. Zhao, and T. Li, "Hysteresis behavior of traditional timber structures by full-scale tests," *Advances in Structural Engineering*, vol. 21, no. 2, pp. 287–299, 2017.

[20] X. Li, J. Zhao, G. Ma, and W. Chen, "Experimental study on the seismic performance of a double-span traditional timber frame," *Engineering Structures*, vol. 98, pp. 141–150, 2015.

[21] F. Vieux-Champagne, Y. Sieffert, S. Grange, A. Polastri, A. Ceccotti, and L. Daudeville, "Experimental analysis of seismic resistance of timber-framed structures with stones and earth infill," *Engineering Structures*, vol. 69, pp. 102–115, 2014.

[22] H. Tanahashi and Y. Suzuki, "Elasto-plastic Pasternak model simulation of static and dynamic loading tests of traditional wooden frames," in *Proceedings of the 11th World Conference on Timber Engineering*, pp. 3309–3318, Trentino, Italy, June 2010.

[23] E. Poletti, A. Dutu, N. Ruggieri et al., "Historic timber frame structures: a comparison of different constructive systems and their resistance to seismic actions," in *Proceedings of 4th International Conference on Structural Health Assessment of Timber structures*, Istanbul, Turkey, September 2017.

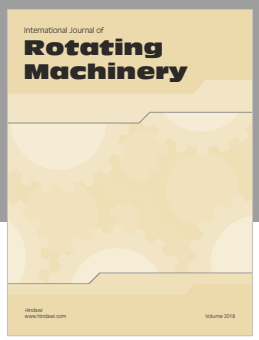

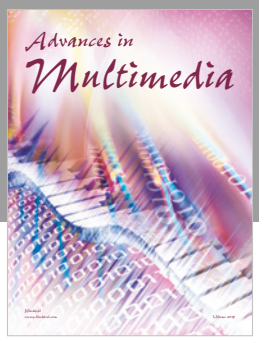

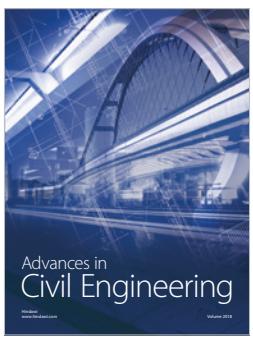

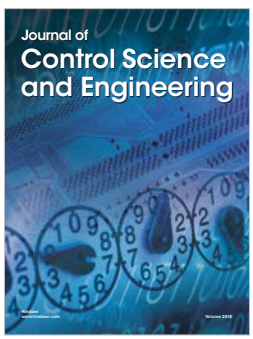

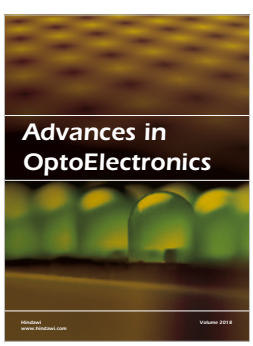

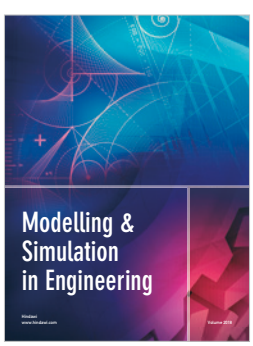

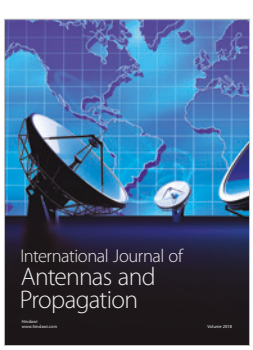

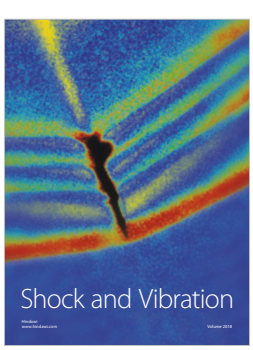

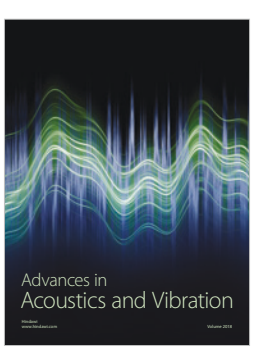

Hindawi

Submit your manuscripts at
www.hindawi.com